remote sensing

MDPI

Article

Characterization of Turbulence in Wind Turbine Wakes under Different Stability Conditions from Static Doppler LiDAR Measurements

Valerie-Marie Kumer, Joachim Reuder * and Rannveig Oftedal Eikill

Geophysical Institute, University of Bergen and Bjerknes Centre for Climate Research, Allegaten 70, 5007 Bergen, Norway; valerie.kumer@gmail.com (V.K.); rannveig.eikill@student.uib.no (R.O.E.)

* Correspondence: joachim.reuder@uib.no; Tel.: +47-55-58-84-33

Academic Editors: Charlotte Bay Hasager, Alfredo Peña, Xiaofeng Li and Prasad S. Thenkabail

Received: 5 July 2016; Accepted: 22 February 2017; Published: 5 March 2017

Abstract: Wake characteristics are of great importance for wind park performance and turbine loads. While wind tunnel experiments provided a solid base for the basic understanding of the structure and dynamics of wind turbine wakes, the consequent step forward to characterize wakes is full-scale measurements in real atmospheric boundary layer conditions under different stability regimes. Scanning Doppler LiDAR measurements have proven to be a flexible and useful tool for such measurements. However, their advantage of measuring spatial fluctuation is accompanied by the limited temporal resolution of individual sampling volumes within the scanned area. This study presents results from LiDAR Doppler Beam Swing (DBS) measurements and highlights the potential of information retrieved from a spectral analysis of wake measurements. Data originate from three Windcube v1 and sonic anemometers, collected during the Wind Turbine Wake Experiment–Wieringermeer. Despite the ongoing research on the reliability of turbulence retrievals based on DBS data, our results show wake peak frequencies consistent with sonic anemometer measurements. The energy spectra show rather distinct maxima during stable conditions, which broaden during unstable and neutral conditions. Investigations on the effect of blade pitch on downstream wind speed and turbulence intensity profiles indicate the potential for the development of stability-dependent wind farm control strategies.

Keywords: LiDAR; wind turbine wakes; atmospheric stability; wind energy

1. Introduction

The understanding and appropriate consideration of wind turbine wakes is of vast importance for a wide range of subtasks during the whole life cycle of a wind farm. This includes the turbine layout during the design phase or the estimation of power production and loads during the operational phase. An improved characterization and description of single turbine wakes has therefore a large potential for the development and application of novel control strategies on the park level, with the aim to optimize the farm production and to reduce the load and fatigue of the individual turbines. A corresponding increase in revenue and reduction in installation and maintenance cost over the park life time will be key factors for a further decrease in the Levelized Costs of Electricity (LCoE).

The investigation of different aspects of the structure and dynamics of wind turbine wakes in full scale and under different atmospheric conditions requires flexible remote sensing methods based on SoDAR (Sonic Detection And Ranging) (e.g., [1]), LiDAR (e.g., [2]) or RaDAR (e.g., [3]) technology. During the last decade, in particular, wind LiDAR systems have massively entered the research field of wind energy (e.g., [4–8]). Corresponding applications for turbine wake investigations have so far been focusing on the average wake structure, e.g., for the test and validation of simple wake models

(e.g., [9]), wake recovery and downstream expansion (e.g., [2,10,11]) or wake meandering (e.g., [12]), in dependence of atmospheric stability. While wake measurements with scanning LiDAR systems lead to an increased understanding of wake characteristics inside the Atmospheric Boundary Layer (ABL), their advantage of spatial coverage is accompanied by limited temporal sampling at any one point in space. Therefore, we want to further investigate the capabilities and limitations of simple Doppler Beam Swinging (DBS) measurements that could complement scanning LiDAR measurements with higher sampling rates and smaller sampling volumes at certain positions in the wake. The higher temporal resolution at selected wake locations could be in particular beneficial for a spectral analysis of wind measurements in the wake.

Sathe et al. [13] arrive in their review on turbulence estimation from Doppler LiDAR measurements at the conclusion that DBS measurements have to be interpreted carefully for the derivation of turbulence statistics, mainly due to the assumption of homogeneous flow at the positions of the four consecutive beam swings and the cross-contamination problem. The cross-contamination problem is related to the wind vector retrieval, which is originally based on the oversampling of wind vectors, but can be avoided if only one wind vector per measurement circle is further analyzed [14]. To avoid the assumption of homogeneous flow during one measurement cycle, the tendency is to go for multiple LiDAR approaches, measuring the wind vector at the same points in time and space. However, this requires the purchase of three LiDAR systems and a rather complex measurement design and data processing. Mann et al. [15] and Fuertes et al. [16] find good agreement with sonic measurement using the multi LiDAR approach. Fuertes et al. [16] further show that, for frequencies greater than 0.1 Hz, the LiDAR probe volume averaging effect becomes significant as the level of energy starts to drop below the sonic reference measurements. Therefore, the interpretation of turbulence from multi-LiDAR measurements at frequencies higher than 0.1 Hz is still challenging.

Despite the assumption of homogeneous flow, DBS measurements have shown their potential for studying wake characteristics, such as horizontal velocity deficits, increased turbulence levels and wake rotation [14,17,18]. Lundquist et al. [19] present DBS measurement errors, by simulating DBS measurements with a large eddy simulation model, in the order of $2\,\mathrm{m{\cdot}s^{-1}}$ and $1\,\mathrm{m{\cdot}s^{-1}}$ in the near-wake region and further downstream at distances greater than three rotor Diameters (D). However, model uncertainties are not taken into account, and the simulated wind vector retrieval still includes cross-contamination effects. Lundquist et al. [19] conclude that the accuracy of DBS wake characterization can be increased by the use of additional reference measurements.

In this study, we want to highlight the performance of processed DBS measurements for the characterization of wind turbine wakes and focus on an analysis in the frequency domain. By processing the DBS data as described by Kumer et al. [14], we show that the cross-contamination effect can be largely eliminated, and LiDAR turbulence spectra are in good agreement with sonic anemometer measurements in free-stream and wake conditions. Wake spectra show peak frequencies in the range of 0.02 to 0.07 Hz, which is in the proximity of the eigenfrequencies of offshore floating wind turbines. Especially during stable conditions, this frequency signature can be of particular interest for offshore floating wind farms, as, e.g., the Hywind Scotland Pilot Park [20].

The manuscript is structured as follows. Section 2 describes the measurement campaign and gives a short introduction to the basic data processing. The results of the data analysis are presented and discussed in Section 3, including a general flow characterization of the experimental site (Section 3.1) and an investigation of the average structure of a single turbine wake based on the profiles of the normalized mean wind speed and turbulence intensity (Section 3.2). Spectral characteristics of the flow field inside the wake are analyzed both in the form of a case study (Section 3.3) and as averages over the whole experimental period as a function of atmospheric stability (Section 3.4). Section 4 provides a final discussion and a short outlook.

2. Materials and Methods

2.1. Measurement Campaign

The dataset analyzed in this study was collected during the WINd Turbine Wake EXperiment –Wieringermeer (WINTWEX-W) [18], a collaborative measurement campaign between the University of Bergen, Christian Michelson Research and the Energy Center of the Netherlands (ECN). The campaign took place at ECN's Wind Turbine Test Site Wieringermeer [21] and was designed to study a single turbine wake of one of the 2.5 MW Nordex research turbines by static and scanning Doppler LiDAR measurements. The Nordex N80 turbines have a rotor diameter and hub height of 80 m and are located on farm land 5 m below sea level. In addition to some farm houses, other prototype wind turbines and meteorological masts disturb the larger-scale flow around our turbine of interest (WT6). The test site location, as well as the measurement set up are pictured in Figure 1. This study is based on wind measurements from three Leosphere Windcube v1, marked by colored squares, and two sonic anemometers mounted on top (108 m) and at hub height (80 m) on the met-mast (M3), marked as a yellow triangle in Figure 1. The black square further downstream, at around 12 D, indicates the position of a scanning wind LiDAR system (Leosphere Windcube 100S) that has, however, not been included in this study. The three Windcube v1, named by their serial numbers as wls37, wls65 and wls67, were orientated along the wake center line for the main wind direction of south-westerly winds (227°). For this setup, the upstream LiDAR (wls67, blue mark) is located at a distance of 3.2 D in front of WT6; the Windcubes in the wake are situated at 1.8 D (wls37, red) and 3.5 D (wls65, green) downstream. A more detailed description of the different expected wake locations with respect to the incoming wind direction can be found in Table 1.

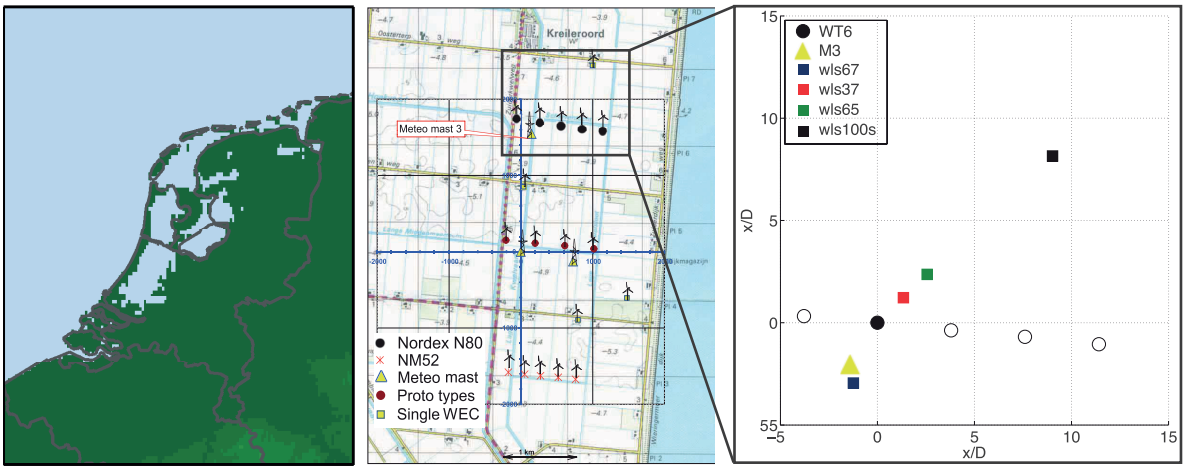

Figure 1. Map of the Netherlands with the location of the wind turbine test site Wieringermeer and the measurement setup. Blue, green and red squares and the yellow triangle indicate the location of the Windcube v1 and the met-mast relative to the research turbine WT6 illustrated by a full circle. Open circles show the rest of the research turbines.

The profiling LiDARs performed standard DBS measurements with four Line-Of-Sight (LOS) measurements at 0°, 90°, 180° and 270° from north, an elevation angle of 60° and a sampling rate of 1 Hz at ten different altitudes (40, 52, 60, 80, 100, 108, 140, 120, 160, 200 m). The range gates centered at 52 and 108 m are set to match the measurement heights of the met-mast and are overlapping with neighboring range gates since the range gate size was 20 m. It should be mentioned that the sampling time interval of the Windcube wls37 was 1.273 s and with that, 0.273 s longer than the sampling interval specified by the manufacturer. The analyzed period includes data from 30 November 2013 to 10 May 2014.

Table 1. Location of the three Windcubes v1 used in this study with respect to expected wakes of the different Wind Turbines (WT5 to WT9) and the Met-mast (M3). The table presents the distance to the corresponding obstacle in rotor Diameters (D) related to the most affected wind direction. The information related to Wind Turbine Number 6 is highlighted in bold letters.

Instrument	Shadow Mast Shadow	Distance (D) 0	Direction (°) 180
M3	WT5	3.5	315
	WT6	**2.5**	**31**
	WT7	5.4	71
	WT8	9.0	81
	WT9	12.7	85
wls67	M3	0.8	357
	WT5	4.2	322
	WT6	**3.2**	**23**
	WT7	5.7	63
	WT8	9.1	76
	WT9	12.8	81
wls37	WT 5	5.2	260
	WT6	**1.8**	**228**
	WT7	2.9	123
	WT8	6.6	107
	WT9	10.3	103
wls65	WT 5	6.7	252
	WT6	**3.5**	**227**
	WT7	3.0	156
	WT8	5.9	121
	WT9	9.5	111

2.2. Data Processing

In the first step, the raw 1 s DBS data of the Windcube v1 had to be de-spiked and filtered due to highly variable data quality, in particular in the case of the wls65. Time periods with strongly variable Carrier-to-Noise Ratios (CNR) were removed from the dataset by filtering for time periods without a registered wiper count. The CNR fluctuations occurred also for levels above −23 dB, which are typically accepted for reliable measurements by the manufacturer. As the remaining raw wind data still included single non-physical spikes, an advanced de-spiking routine was developed and applied. Spikes were detected as outliers if located outside of four standard deviation (4σ) based on a 15 min averaging interval. Since the data were partly collected in highly turbulent wake conditions, we kept measurements exceeding 4σ, if the exceedance persisted over more than 15 consecutive measurements. After repeating this algorithm four times, the performance of the de-spiking routine was manually checked for each measurement day. A more detailed description of the detected data quality issues and the de-spiking algorithm can be found in Eikill [22].

After the de-spiking, we turned the coordinate frame into the meteorological convention and additionally filtered the DBS data for independent wind vectors to avoid the misleading oversampling of wind vectors in their retrieval algorithm. Using only every 4th retrieved wind vector leads to an independently sampled time series, compared to the original time series, where one LOS measurement is used up to four times in the wind vector retrieval process. By filtering the data to use only independent wind vectors, the potential effects of cross-contamination described by Sathe et al. [23] can be avoided. Therefore, every 4th wind vector was taken into account, leading to a sampling interval of 4 s, as described by Kumer et al. [14].

After filtering the data, spectral energy densities were calculated for one- and four-hour periods in the later presented composites and case studies, respectively. Following Kumer et al. [14], we linearly

interpolated the data on a regular time grid and turned the coordinate system into the mean wind direction before calculating the spectral energy density $S(f)$ (Equation (1)).

$$S(f) = \frac{2 * |F(f)|^2}{\Delta f} \qquad \text{with} \qquad F(f) = \frac{1}{N} \sum_{k=0}^{N-1} (k\Delta t) * e^{2\pi f k \Delta t} \tag{1}$$

$S(f)$ is the one-sided power spectrum as a function of frequency f. It is estimated by splitting the analyzed period up into 20 blocks. A discrete Fourier transform $F(f)$, with time represented as a whole-number multiple k of the sampling rate Δt, is applied on each block, and the results are averaged over all samples in the block. Each block is smoothed with a Hanning window to suppress spectral leakage effects. N is the number of all samples in the analyzed period.

In order to avoid rigorous data interpolation, $S(f)$ was only calculated for periods where fewer than five data points were missing. To illustrate the performance of the spectral energy density retrievals and their differences between the data filtering methods, we show and compare power spectra from LiDAR DBS and sonic anemometer measurements during a free-stream and a wake case (Figures 2 and 3). The comparison is based on the energy spectra of the three stream-wise wind components u (along-wind), v (cross-wind) and w (vertical) and the Turbulence Kinetic Energy (TKE) calculated from sonic anemometer measurements and DBS data processed with different techniques.

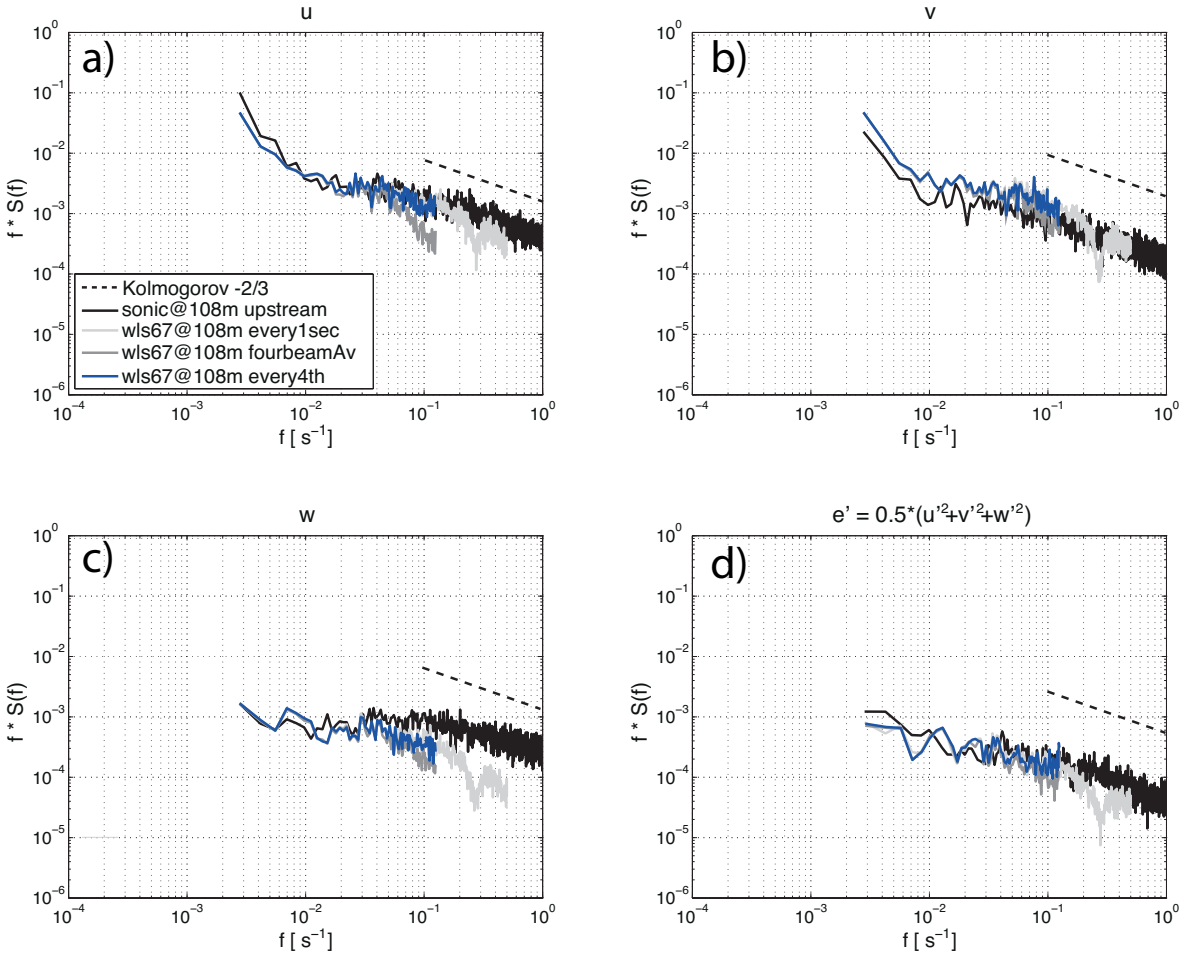

Figure 2. Energy spectra of four hours on 4 March 2014 during free stream conditions ($dir_{mean} = 240°$) of the along-wind (**a**), cross-wind (**b**) and vertical component (**c**) and TKE (**d**). Black colors show data from the sonic anemometer, and blue and grey colors show Windcube wls67 data, all at 108 m. The dashed line indicates the $-2/3$ Kolmogorov slope.

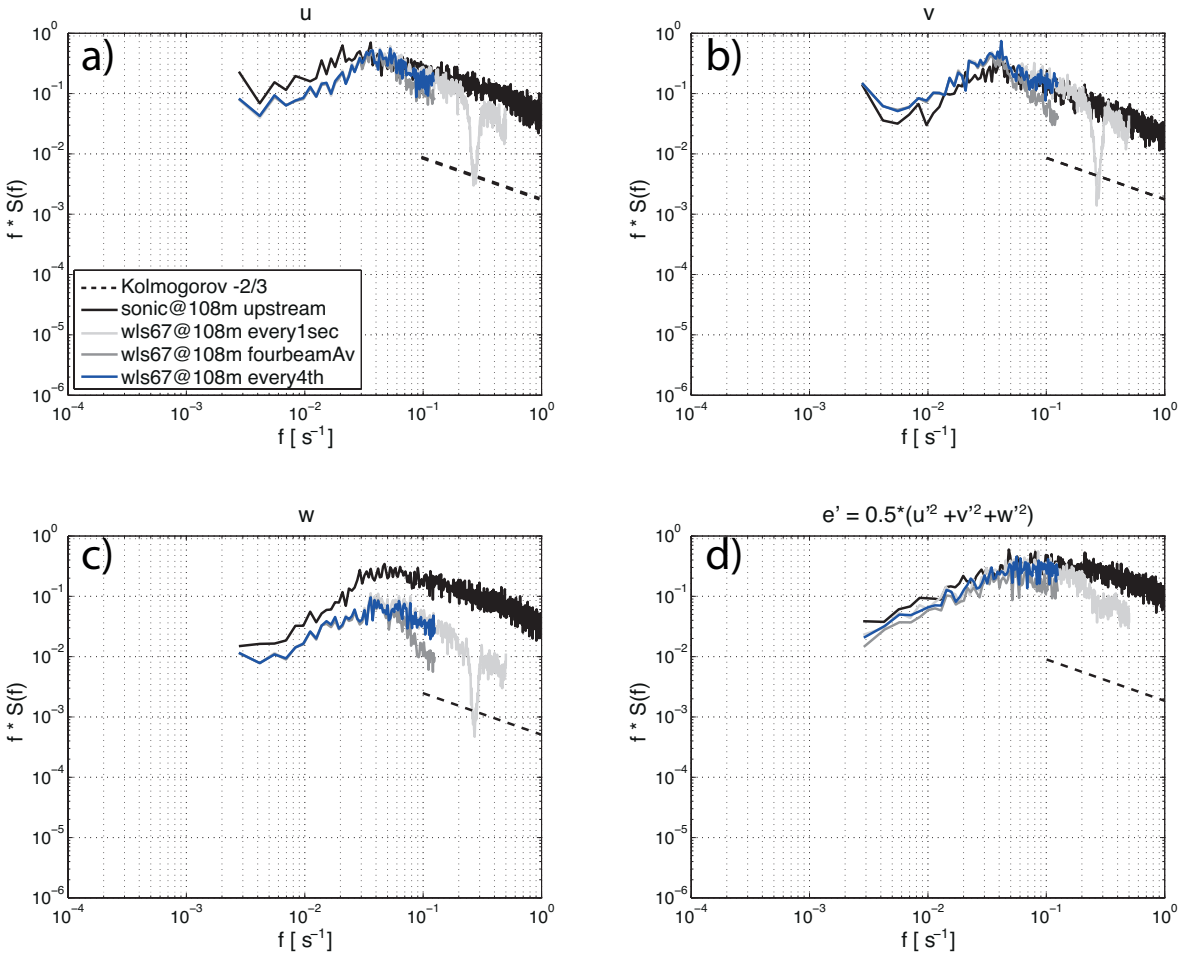

Figure 3. Energy spectra of four hours on 1 March 2014 during wake conditions ($dir_{mean} = 60°$) of the along-wind (**a**), cross-wind (**b**) and vertical component (**c**) and TKE (**d**). Black and blue colors show wake data from the sonic anemometer and Windcube wls67 at 108 m. The dashed line indicates the $-2/3$ Kolmogorov slope.

In the free-stream case, we analyzed a 4 h period from 19 to 23 UTC on 4 March 2014, which was characterized by south-westerly winds turning from 230° to 250° with wind speeds of around 5 m·s^{-1}. The unprocessed DBS data, shown in light gray, underestimate the turbulence spectra compared to the sonic measurements, which was already found and discussed by Canadillas et al. [24] (Figures 2 and 3). Similar to Fuertes et al. [16], the drop in energy for frequencies above 0.1 Hz can be related to probe volume averaging. Following Kumer et al. [14], we averaged all four wind vectors retrieved during one complete measurement cycle, illustrated in dark grey, which filters even more energy out of the flow compared to the unprocessed and sonic data. Finally, we show the spectrum of independent wind vectors, by only taking every fourth DBS measurement, in blue, with the same energy levels as the sonic measurements in the stream-wise wind component and the TKE estimate. Both the sonic and the processed DBS data show an energy decay parallel to the Kolmogorov $-2/3$ slope.

The v- and w-components show, in contrast, distinct differences from the sonic spectra. In the w-component, differences occur both with respect to the overall energy level, which is clearly underestimated by the LiDAR measurements, and the slope of the spectra towards higher frequencies. This behavior is related to the limitations arising from the Windcube v1 measurement setup with only 4 beams, the fact that the vertical wind component is not measured directly and that the probe volume averaging has a larger effect in the vertical, filtering out small-scale turbulence, which is typical for the vertical wind component. In the v-component, energy spectral densities are slightly overestimated

by the LiDAR. One possible error source for the different performance between the v-spectra and the u-spectra is the LiDAR measurement geometry. Dependent on the prevailing wind direction, one of the wind components can be derived from two beams perpendicular to the main flow. Measuring radial velocities with an angle to the mean flow leads to measurement errors, since only parts of the aerosol movements are captured. The larger the angle between the prevailing wind direction and the LOS measurement, the bigger the error. Sathe and Mann [25] give the increased contribution of the spectral tensor component $\Phi_2 2(k)$ as the wave number k goes to 0 as an explanation for the increased spectral energy, but conclude that further research needs to be done.

In the wake case, the period from 00 to 04 UTC on 1 March 2014 is dominated by north-easterly winds turning from 50° to 80° with a wind speed of around 9 m·s^{-1}. Both measurement methods show a distinct maximum in the spectra of the wind components at around 0.03 Hz and a broader, but still increased level of variance in the TKE spectra. While the level of variance is underestimated for the w-component and at the low frequency end of the u-spectrum, the different datasets seem to agree very well in the TKE spectra. The unprocessed and average DBS data show the same features as discussed during the free-stream condition with an energy drop for frequencies larger than 0.1 Hz.

The fact that the v-component seems to be better represented than the u-component in the wake case, can be related to the prevailing wind direction, as the accuracy of the DBS data is dependent on the beam positions relative to the wind direction. Additionally, the position of the LiDAR in the wake is also related to the prevailing wind direction, as sometimes one LOS measurement could be outside the wake, while others are still inside the wake. It should, however, be pointed out that the two measurement systems seem to produce very similar and reproducible spectral energy densities in these free-stream conditions. This provides confidence that qualitative and quantitative estimates of wake effects based on Windcube v1 measurements are possible and justified.

A more detailed analysis of these wake spectra is presented in Section 3 and discussed in the context of other studies in Section 4. In the further analysis of the energy spectra, we also separate the dataset for different atmospheric stability conditions. This turned out to be not straight-forward, as the only available on-site stability information is from temperature difference measurements between 37 m and 10 m at the met-mast. Due to the lack of co-located wind speed measurements at the same heights, the Richardson number cannot be calculated. For the determination of the Obukhov length, necessary to determine the stability parameter z/L, additional heat flux measurements would be required, which were not stored for the sonic anemometers on this met-mast. We therefore had to derive a proxy for the atmospheric stability based on the 10-minute average temperature difference measurements described above.

Assuming a dry adiabatic lapse rate, the local change in temperature over a 27 m height interval should under neutral conditions result in a temperature difference of -0.27 K. Analyzing the temperature difference measurements revealed an offset compared to the theoretical value, which indicates calibration issues. Therefore, we aimed to find an empirical estimate of the measured adiabatic lapse rate that represents the local conditions on site. To do so, we selected night time conditions with high wind speeds (>15 m·s^{-1}) to ensure neutral conditions. Additionally, we adapted the indicators for stable and unstable conditions to fit the whole dataset by analyzing the observed temperature difference distribution over the prevailing wind speeds at 108 m. The resulting stability proxy is presented in Table 2.

Table 2. Definition of the stability criteria.

Stability Class	Temperature Difference	Data Share	Average Wind Speed at 108 m
stable	$dT > 0.03$	27%	9.1 m·s^{-1}
neutral	$-0.26 \leq dT \leq 0.03$	55%	9.8 m·s^{-1}
unstable	$dT < -0.26$	18%	8.9 m·s^{-1}

3. Results

3.1. General Flow Field Characterization

The measurement setup with the wls67 in the close vicinity of the met-mast and its sonic anemometer measurements allows for a detailed site characterization with respect to the quantification of flow distortion and wake effects to be considered for a further analysis of the retrieved wind dataset. For this purpose, we calculated the wind speed ratios from the sonic measurements at 108 m and the wls67 measurements at 100 m on the basis of 10 min averages. The corresponding results are presented in Figure 4.

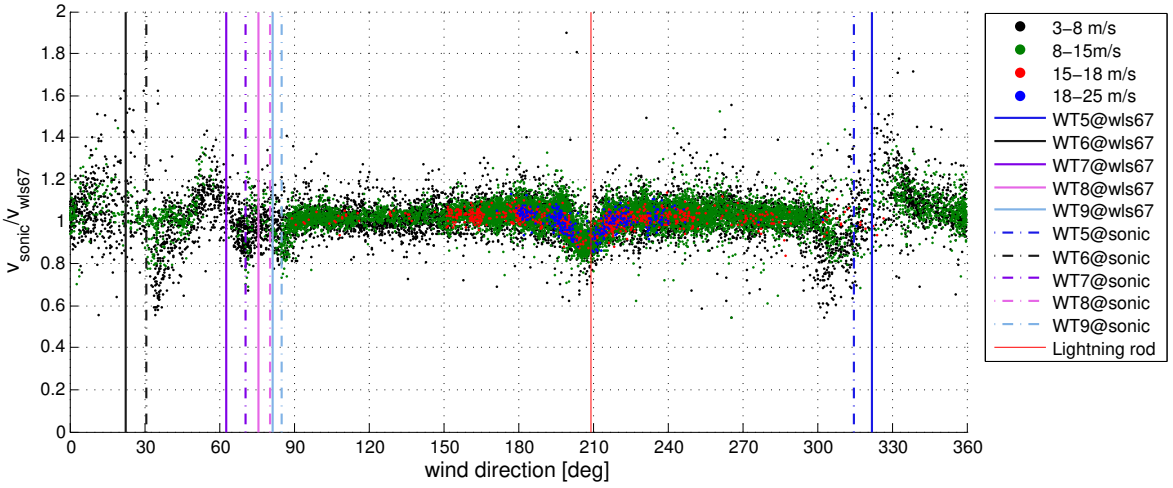

Figure 4. Wind speed ratios between the sonic anemometer measurements on M3 at 108 m and the wls67 measurements at 108 m on the basis of 10 min averages. Different wind speed intervals are color-coded. The vertical red line indicates the effect of a lightning rod on the sonic anemometer measurements. The colored solid and dashed vertical lines mark the position of the expected wake effects of the five test turbines on the wls67 and sonic anemometer measurements, respectively.

It shows in general rather undisturbed conditions in the wind direction interval between 90° and 290°, except for an approximately 30° wide directional band centered around 205°. Here, the sonic anemometer at 108 m on top of M3 is located in the wake of the lightning rod mounted on the opposite pillar of the triangular mast. This leads to a reduction of the wind speed measured by the sonic anemometer of up to 20%. The color coding for the wind speed also shows that the highest wind velocities are clearly occurring for southerly directions and that an increase in wind speed is associated with a distinct reduction in the spread of the calculated wind speed ratios. For wind directions from 0° to 90° and 290° to 360° the wind speed ratios clearly indicate the complex influence of the different turbine wakes on both sonic and LiDAR measurements, with very clear signals from the nearest turbines WT5-WT7 and more diffuse footprints of the turbines WT8 and WT9. The sector between 100° and 150° shows the lowest level of variability in the wind speed ratios and seems to be closest to free-stream conditions. However, also the wind direction range of 227° $\pm$ 10° seems to be rather undisturbed and therefore well-suited for the analysis presented in the following sections.

3.2. Average Wake Profiles

In a first step, the measurements of the three static Windcube have been analyzed with respect to average wind speed and turbulence intensity (TI) profiles for different atmospheric stability conditions. As the LiDARs are aligned for the main direction, we further filtered for the wind direction interval 217° to 237° and for the situations where the wind turbine was producing power. Before averaging over the resulting cases, we normalized the wind speed profiles by the corresponding 80 m value of

the upstream LiDAR wls67 (Figure 5). This allows for a direct comparison of the average wind speed deficit in the wake region.

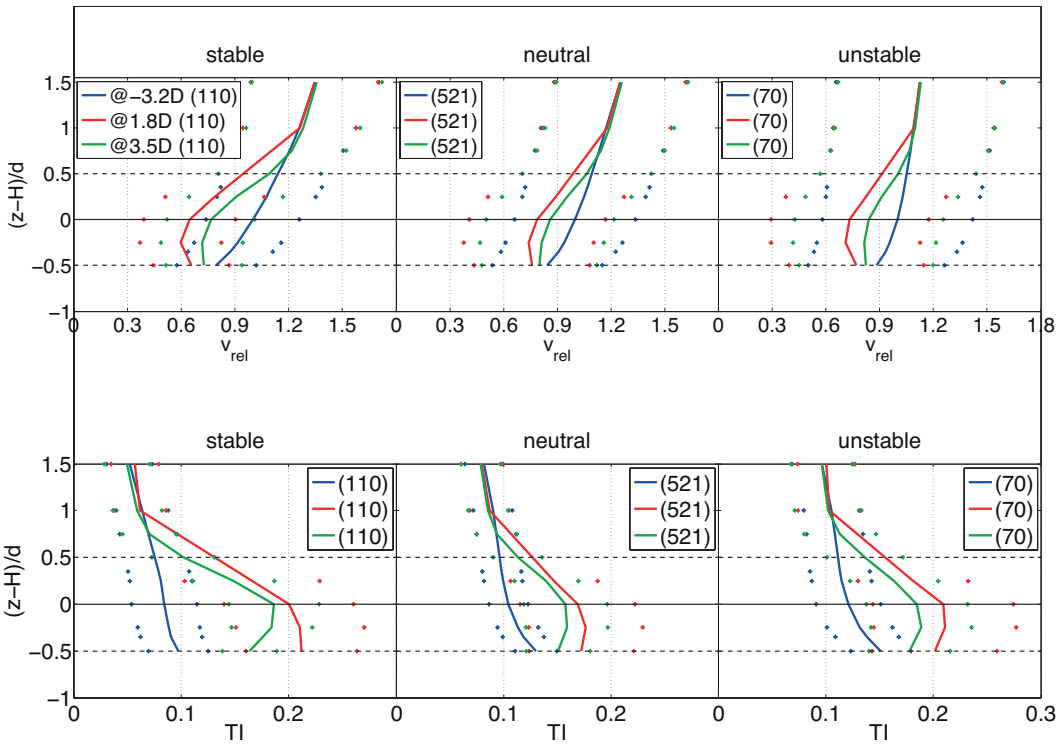

Figure 5. Mean normalized profiles of wind speed v_{rel} (upper panels) and turbulence intensity TI (lower panels) filtered for the different stability classes and averaged over all cases in the wind direction interval 217°–237°. The individual 10 min average wind speeds of all three LiDAR systems have been normalized by the corresponding 80 m value of the upstream LiDAR wls67 before averaging over the number of available profiles indicated in the legend. Dots indicate the standard deviation at each measurement altitude before the normalization.

The inflow wind profiles measured by the wls67 show the expected logarithmic wind profile for neutral conditions and a distinct increase (decrease) in wind shear for stable (unstable) conditions. The profiles measured inside the wake by the wls37 and wls65 reveal a distinct wind speed reduction, both depending on atmospheric stability conditions and downstream distance from the wind turbine. Figure 5 illustrates that the decrease in horizontal wind speed is significantly larger for stable cases than for both unstable and neutral situations. The wake deficit reaches its maximum at an altitude of 60 m, i.e., slightly below hub height. At this height, the velocity deficit reaches 40% and 30% at a distance of 1.8 D downstream in stable situations and neutral or unstable situations, respectively. Further downstream at 3.5 D, the wake has already recovered to a velocity deficit of 30% (stable) and 20% (neutral and unstable). For stable conditions, the measured deficits at 1.8 D and 3.5 D are in good agreement with the results presented by Aitken et al. [10], while velocity deficits under neutral or unstable conditions are slightly below the reported ones. The strongest deficits are not only described by the average profiles, but also by the measured standard deviations.

In general, the standard deviation of the wind profiles is increasing with height, which is related to the increasing horizontal probing area that is scanned during one measurement cycle. Especially during unstable conditions, where horizontal flow variations are common, the standard deviations are the largest. Furthermore, the vertical wake expansion is fairly similar during stable and neutral atmospheric stratification, as compared to a slightly higher expansion during unstable conditions.

Wake deficits reach an altitude of 160 m at 1.8 D, which decreases to about 120 m for measurements taken further downstream at 3.5 D. This is somewhat unexpected, as wake models in general predict a wake expansion also in the vertical (e.g., [26]). The location of the wls65 seems to be far enough downstream so that mixing of the shear layer above the rotor disk is already reducing the vertical wake extension. This reduction is in accordance with findings by Iungo et al. [27] from scanning LiDAR wake measurements downstream of a single Enercon 2-MW wind turbine, performed in Switzerland. They reported a steep increase of the wake region right behind the turbine, reaching 0.8 D above the hub height at a distance of 1 D downstream. With increasing distance downstream, the vertical wake extension decreases to about 0.5 D above hub height at a downstream distance of 3.5 D, which is in excellent agreement with our measurements.

The lower panels in Figure 5 show expected upstream turbulence intensity (TI) profiles with values increasing towards the ground, which are in accordance with measurements from the German Research Platform FINO1 presented by Emeis [28]. Also in agreement with Emeis [28], the overall TI values are lowest in stable stratification. At hub height, the average TI values reach 0.08 for stable, 0.10 for neutral and 0.12 for unstable stratification. The profile for stable conditions shows a more or less linear decrease with height, while both neutral and unstable conditions indicate distinctly enhanced TI values for the lowest measurement heights. This could be associated with additional production of turbulence towards the ground, caused mainly by shear for the neutral atmosphere and by buoyancy effects in unstable conditions.

The LiDARs situated in the wake of WT6 exhibit a large increase in turbulent activity, with maximum values of TI at hub height and below. The increase of TI is a combined effect created by the turbine structure, the rotating blades and the reduction in average wind speed in the wake. As for the average wind speed profiles, the wake effect on TI is also most pronounced for stable conditions, increasing upstream TI levels at hub height from 0.08 to 0.20 and 0.18 at 1.8 and 3.5 D downstream, respectively. The lowest average TI values in the wake are observed during neutral conditions with 0.17 and 0.15 at 1.8 D and 3.5 D downstream, respectively.

Determining the vertical wake expansion by the TI profiles leads for the 1.8 D downstream distance of the wls67 to a similar result as using wind speed deficits (160 m). The TI data from the wls65, measuring further downstream in the wake at 3.5 D, show in contrast a larger vertical wake extension from the TI estimate, reaching altitudes closer to 150 m rather than the 120 m resulting from the wind speed profiles. The higher wake extension in TI goes along with the above-mentioned shear line that entrains ambient air from aloft into the wake, leading to enhanced mixing and with that, higher TI values in this region. In general, the location of the shear line between blade tip height and undisturbed air aloft can introduce measurements errors in the collocated ranged gate, due to probe volume averaging.

Similar to the standard deviation of the wind profiles, unstable conditions show the largest standard deviations in the TI profiles. The relative increase from standard deviations up- and down-stream of the wind turbine is larger than for the wind profiles.

A way to possibly reduce the enhanced turbulence in wakes is by the intentional increase of blade pitch angles; especially in stable cases, where TI values are highest and wind speeds are mostly below rated wind speed with non-active blade pitching. An earlier pitch control could potentially improve the wake recovery as illustrated for normalized wind and turbulence profiles under different blade pitch angles in Figures 6 and 7.

Figures 6 and 7 show that even very small changes in the blade pitch angle have large effects both on the average wind speed and TI profiles. The largest wind speed deficits reduce from 40% to 20% for blade pitch angles greater than 3°. Similarly, the largest TI values reduce from 24% to 15%. The effect seems to be consistent over all measurement heights. This information could in the future be beneficially applied to develop stability and wind speed-dependent wind farm control strategies.

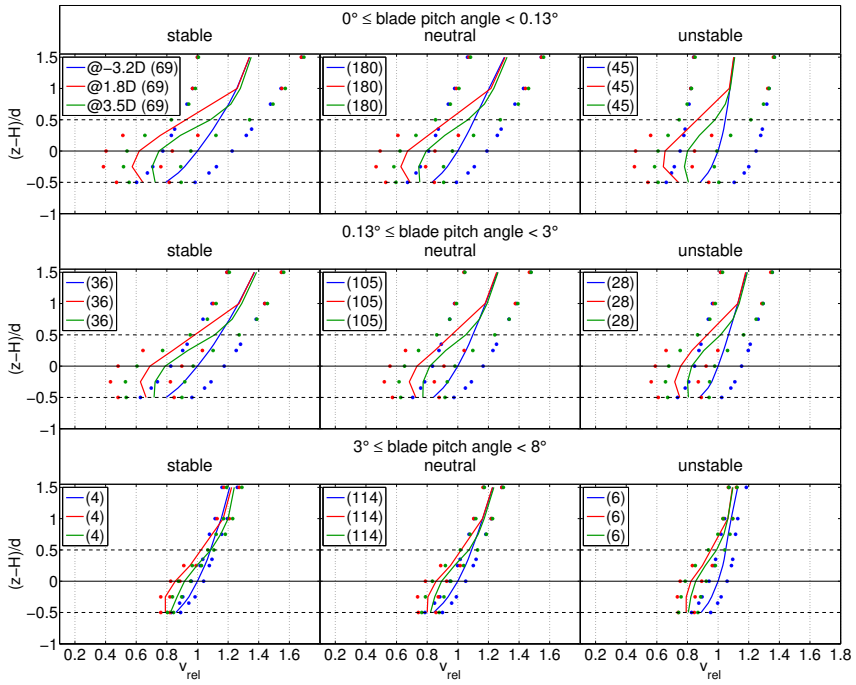

Figure 6. Mean normalized profiles of wind speed v_{rel} filtered for pitch angles between 0° and 0.13° (top), 0.13° and 3° (center) and 3° and 8° (bottom), wind directions between 217° and 237° and different stability classes. The individual 10-min average wind speeds of all three LiDAR systems have been normalized by the corresponding 80-m value of the upstream LiDAR wls67 before averaging the number of available profiles indicated in the legend. Dots indicate the standard deviation at each measurement altitude before the normalization.

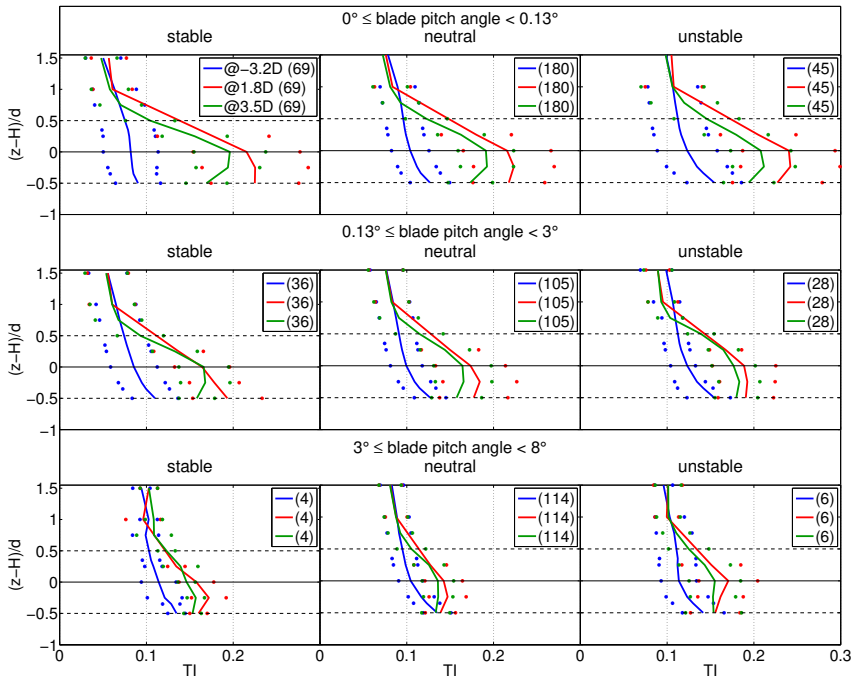

Figure 7. Mean profiles of TI filtered for pitch angles between 0° and 0.13° (top), 0.13° and 3° (center) and 3° and 8° (bottom), wind directions between 217° and 237° and different stability classes. Dots indicate the standard deviation at each measurement altitude. The legend includes the number of averaged profiles.

3.3. Case Study of the Spectral Signature of a Turbine Wake

In order to look at frequency signatures of the above averaged time series, we calculated spectral energy densities of the three wind components as well as for the raw TKE estimate. The LiDAR spectra are derived from processed DBS raw data, as described in Section 2. By comparing LiDAR spectra to spectra from sonic anemometers, we found that Windcube v1 measurements can qualitatively represent turbulence spectra of the atmospheric boundary layer up to the frequency of 0.125 Hz. Spectral energy densities of TKE are well represented in free-stream and wake conditions, while the agreement in the spectra of the horizontal wind components is dependent on the wind direction and beam locations; spectra of the vertical component are underestimated (Figures 2 and 3).

To highlight the difference between upstream and downstream spectra, we analyzed a four-hour period from 19:00 to 23:00 UTC on 4 March 2014. During the selected period, south-westerly winds from around 230° dominated with an average horizontal wind speed of around 5 $m \cdot s^{-1}$ at hub height. The measured wind speeds are below the rated wind speed of the Nordex research turbines, meaning that the blades are blocking most of the flow without an increased pitch angle. Typically, for winter night-time conditions, the atmosphere was stably stratified, prohibiting vertical mixing and allowing longer life times of disturbances. Under these conditions, the Windcube wls67 and the met-mast are upstream of the research turbine WT6, and the Windcubes wls37 and wls65 are located downstream inside the wake.

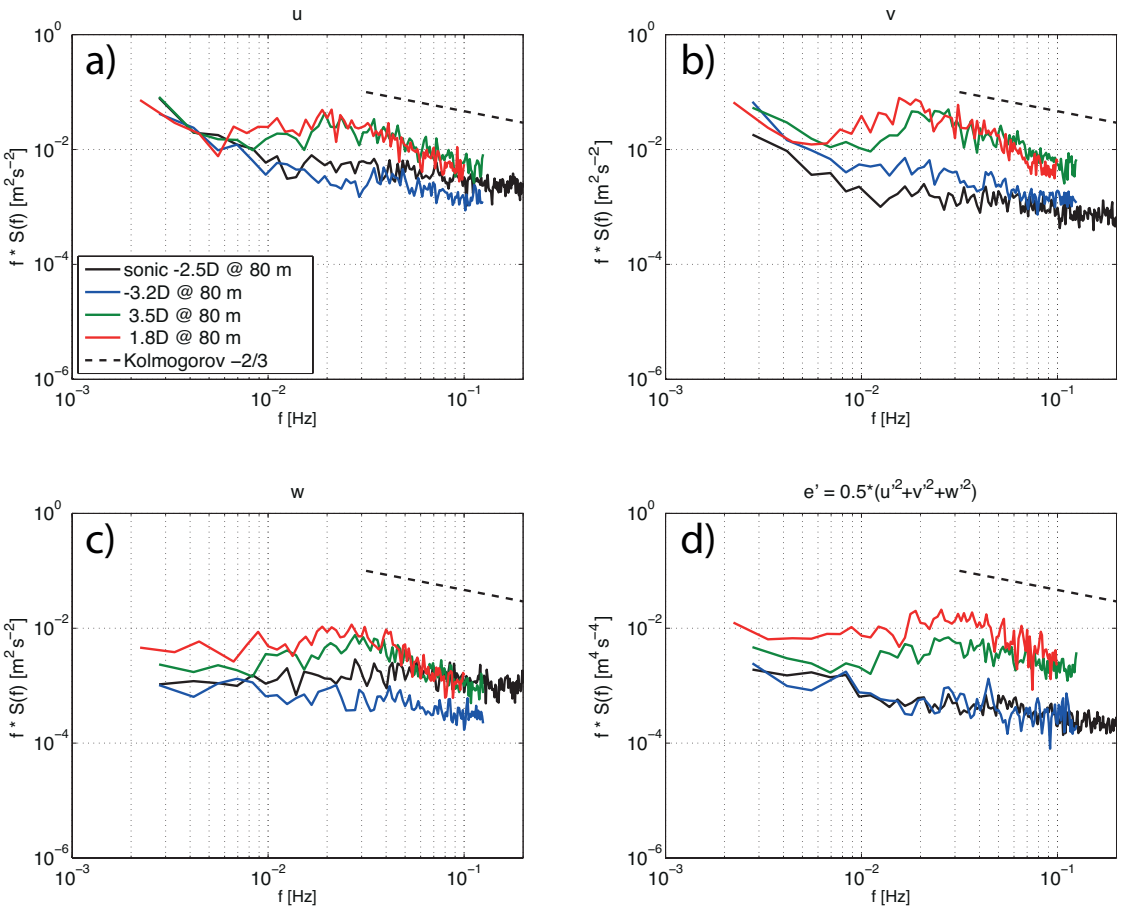

Figure 8. Energy spectra of four hours on 4 March 2014 in free stream (blue and black) and wake conditions (green and red) of the along-wind (**a**), cross-wind (**b**) and vertical component (**c**) u, v, w and TKE (**d**). Black colors show data from the sonic anemometer and blue; red and green colors show Windcube wls67, Windcubes wls37 and wls65 data at 80 m (hub height). The dashed line indicates the −2/3 Kolmogorov slope.

When comparing the turbulence spectra of the free-stream to the wake conditions, a clear maximum at around 0.02 Hz becomes visible in the spectral energy densities of the along-wind component u at hub height (Figure 8). The maximum in u goes along with an increased level of turbulence in the other wind components, as well as in the TKE estimate. Although the vertical component is not accurately represented in the four-beam Windcube v1 data, the relative differences between the two Windcube instruments can be seen as a qualitative indication of variances in the vertical wind speed. These differences in vertical wind speed fluctuations seem also to influence the variance in TKE. The level of variances in TKE is decreasing for the wls65, located further downstream.

Above blade tip height (at 160 m), the distinct maximum in the spectra disappears, but the level of variance is still elevated. In contrast to the observed wind spectra (Figure 9a–c), the spectra of TKE (Figure 9d), which represents the sum of squared variances of the three wind components, show a still visible wake signature. At the presented measurement height, the spectral energy density of TKE is highest at 3.2 D downstream. Due to the measurement height above the blade tip and the horizontal wake expansion, the LiDAR beams of the Windcube located closer to the turbine are outside of the rotor swept area, while those of the Windcube further downstream are inside the expanded area. Therefore, the variance of TKE is highest further downstream. This effect is obliterated for the averaged profiles presented above, as the rotor swept area moves in and out of the LiDAR beam geometry for the selected wind direction sector.

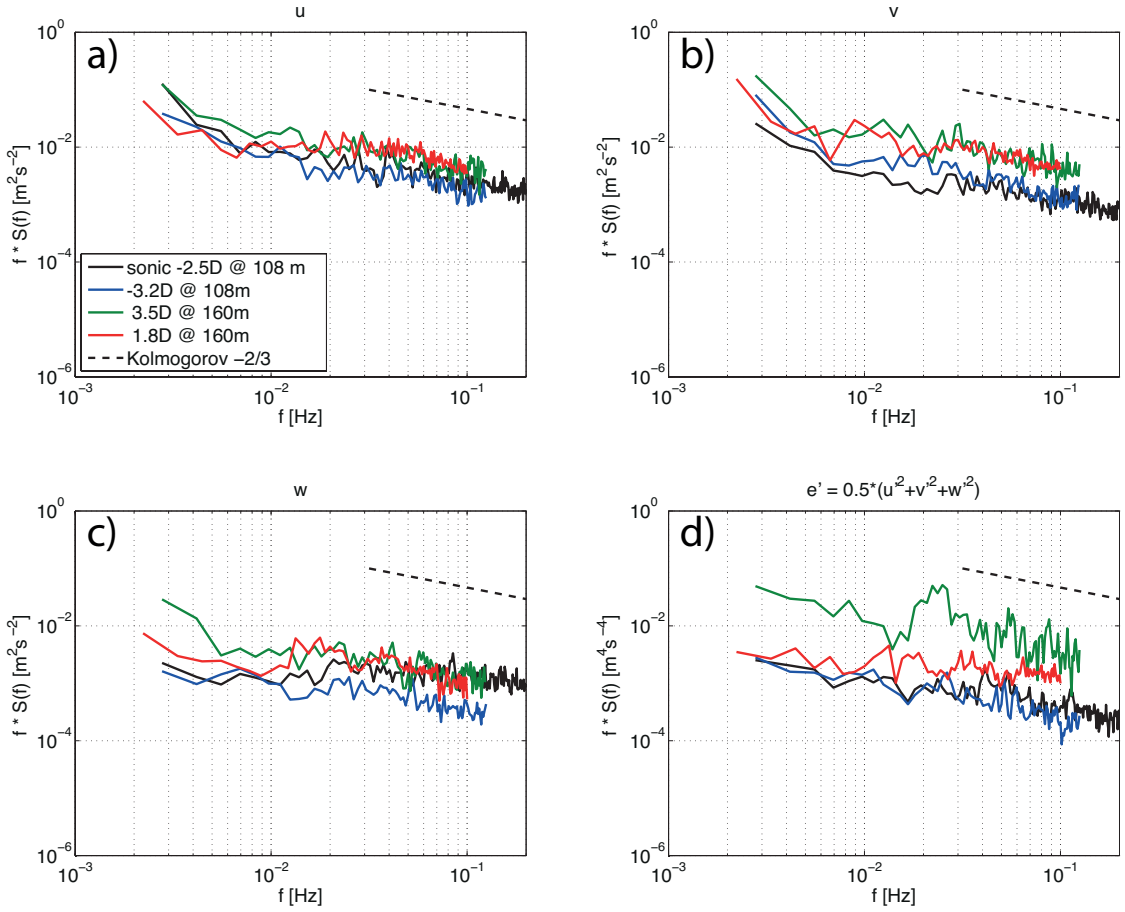

Figure 9. Energy spectra of four hours on 4 March 2014 in free stream (blue and black) and wake conditions (green and red) of the along-wind (**a**), cross-wind (**b**) and vertical component (**c**) u, v, w and TKE (**d**). Black and blue colors show data from the sonic anemometer and Windcube wls67 at 108 m; red and green colors show Windcubes wls37 and wls65 data at 160 m. The dashed line indicates the −2/3 Kolmogorov slope.

3.4. Effects of Stability on Turbulence Spectra in Wakes

For a better understanding on how the atmospheric stability, wind direction and with that wake position, in terms of LiDAR locations, are influencing the wake spectra, we calculated hourly spectral energy densities for the five-month period. The hourly spectra were binned and averaged over a 10° wind direction and 0.0066 Hz frequency intervals.

The maximum in the u-spectra of the wls37 and wls65 is still visible after averaging and normalizing the data with average wind speed for stable conditions occurring during the whole measurement period and plotting the 210° to 220° bin in Figure 10. Interesting to see is that the upstream u-spectra also show a broad maximum and an elevated level of variance. The increase in variance in the upstream u-spectra can be explained by wake effects from a turbine located 1 km south-southwest and from prototype turbines with lager rotor diameter located 2 km south of wind turbine WT6. The maxima of the spectra seem to shift towards higher frequency with increasing downstream distance. The maxima in the upstream spectra are not present in the case study illustrated in Figure 8, either due to the operational status of the other turbines or due to averaging over the selected wind direction sector. A further investigation of the effect is not possible due to the lack of information on the operational status of those other turbines.

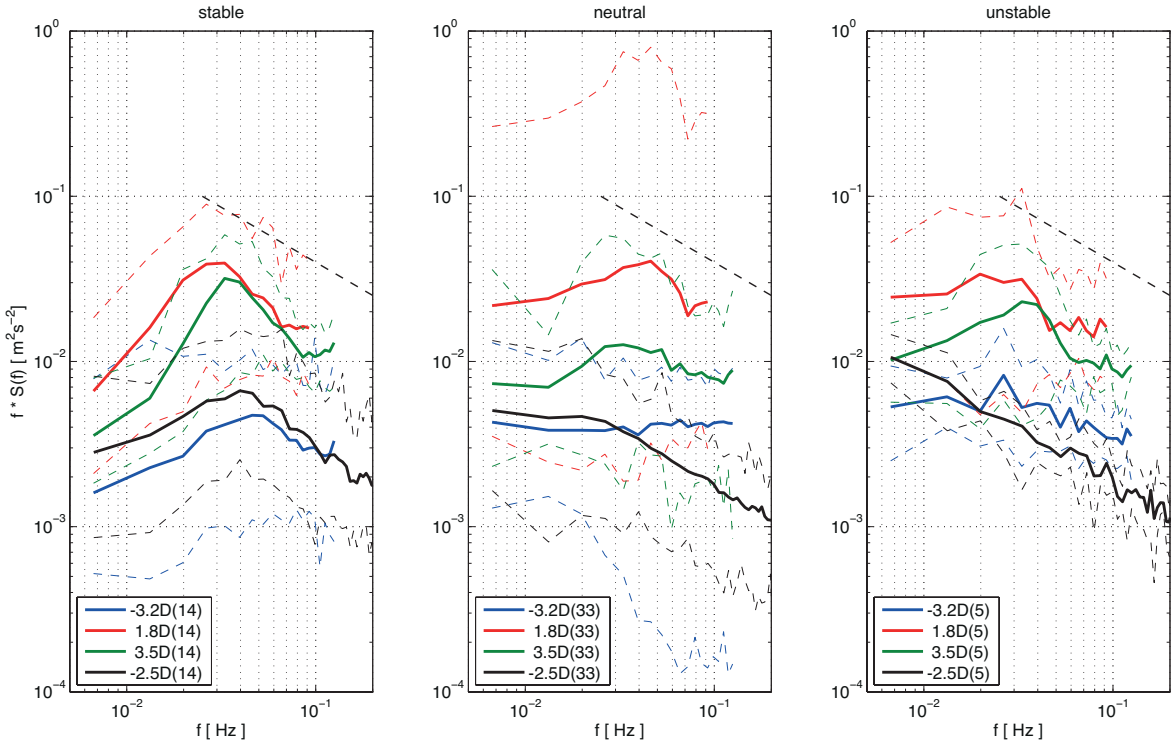

Figure 10. Composites of normalized hourly energy spectra u/u_{mean} at 80 m for wind directions between 210° and 220° under stable (left), neutral (center) and unstable (right) conditions. Dashed lines show maximum and minimum values of the data bin. Data from the upstream sonic and Windcube wls67 are illustrated in black and blue, while downstream Windcubes wls37 and wls65 are illustrated in red and green, respectively. The legend shows additionally the number of averaged hours in parentheses. The thick dashed line indicates the $-2/3$ Kolmogorov slope.

Comparing the neutral and unstable cases to the stable cases, the spectra start with an overall higher variance level, but the relative increase of variance introduced by the wake is lower than in the stable cases. During neutral and unstable conditions, mixing of undisturbed air into the wake is increased and more effective, leading to a faster wake recovery. Due to mixing in the neutral case, the distinct wake maximum of the wls37 and wls65 broadens and shifts towards higher frequencies. In

the unstable cases, the wake spectra start to recover to upstream conditions and almost follow the Kolmogorov $-2/3$ slope at the high frequency end of the spectra. Upstream spectra are free from wake disturbances, as seen in stable cases.

The spread, between the mean of the wind direction bin and its maximal and minimal members, indicates the sensitivity between the wake and beam location in dependence of the prevailing wind direction. The spread is biggest during neutral conditions. Furthermore, during neutral conditions, the slopes of the DBS spectra are less steep compared to the sonic spectra and stop following the Kolmogorov $-2/3$ slope, which could be an averaging effect. Furthermore, measurement errors associated with the beam location could be strongest during neutral conditions where wind speeds are highest.

In order to see the evolution of these wake maxima for different wind directions and therefore different upstream conditions and wake positions, Figure 11 shows the composite of all u-spectra in consecutive wind direction bins for all three Windcube. As a reference to the wls67 data, u-spectra composites of the sonic measurements are also included. Dependent on the wind direction, the sonic anemometer and the Windcube experience free-stream or wake conditions due to the different locations with respect to one of the five research turbines. The positions in relative rotor diameters for the different directions are summarized in Table 1.

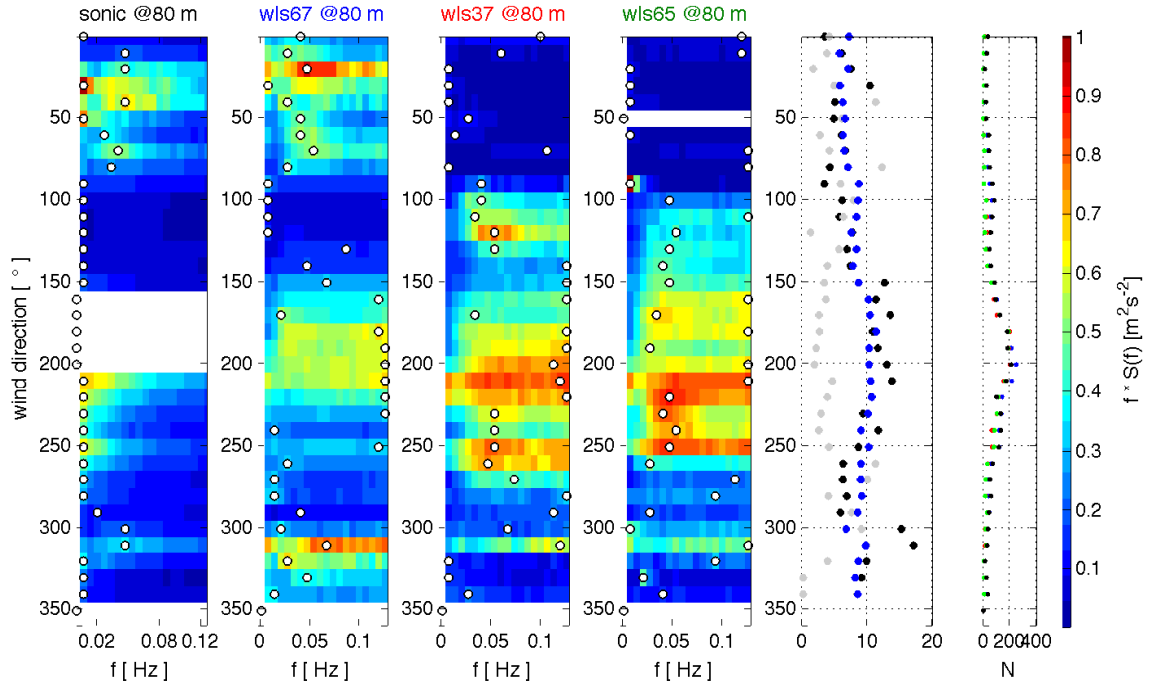

Figure 11. Composites of hourly energy spectra of u at 80 m for all wind direction bins from wls67, wls37 and wls65 (from left to right). White circles indicate the maximal spectral energy density of each direction bin. Additional subplots show wind direction bin averaged horizontal wind speeds at 108 m (blue in ($m \cdot s^{-1}$)), power output (black in (MW/100)) and blade pitch angle (gray in (°)) of wind turbine WT6 and the number of averaged hours in each bin for wls67 (blue), wls37 (red) and wls65 (green).

Figure 11 presents composites of the spectral energy density of the along-wind component for 10° wind direction bins. Northerly wind directions place the Windcube wls67 downstream of the research turbine row, while for southerly winds, the Windcubes wls37 and wls65 are located downstream and affected by the wakes. This upstream or downstream location of the LiDARs is clearly visible in the u-spectra with increased levels of variance and wake peak frequencies fluctuating around 0.02 and 0.05 Hz in different wake positions. In the case of south to south-westerly winds, the upstream measurements of the wls67 are disturbed by far-wake effects of the further upstream prototype wind

turbines. Nevertheless, the level of variance still increases for the downstream LiDARs wls37 and wls65 in these conditions. Distinct maxima are only visible in the wls65 data furthest downstream.

In addition to the u-spectra, the power production and blade pitch angle of wind turbine WT6 and the horizontal wind speed of the sonic anemometer at 108 m are also available and averaged over the same wind direction bins. Easterly and westerly winds show the lowest production of turbine WT6 since it is operating in the wake of turbine WT9 or turbine WT5, respectively. Maximum production seems to be linked to north-westerly winds coming from offshore and passing only a short distance over land before reaching the turbines. However, less data are available for these wind directions.

Filtering the hourly u-spectra presented in Figure 11 with respect to the prevailing atmospheric stability conditions (see Table 2) allows for a more detailed discussion of the wake peak frequency. The above presented hypothesis of consistent wake maxima over long distances under stable conditions, the shifted wake maxima towards higher frequencies under neutral conditions and the faster wake recovery under unstable conditions, seems to be consistent over all wind direction bins (Figures 12 to 14).

Stable conditions are generally characterized by lower wind speeds and blade pitch angles, resulting in the lowest levels of variance, but rather distinct maxima indicated by the white dots in the composites (Figure 12). Peak frequencies vary between 0.03 and 0.05 Hz in almost all bins associated with a turbine wake. In neutral conditions, wind speeds are generally higher, leading to high variances in the u-spectra (Figure 13). Wake peak frequencies tend to shift towards higher frequencies. For south-westerly winds, wind speeds are highest, resulting in the highest power production, which shows that the turbine row was clearly designed for those conditions. In unstable conditions, southerly variances are reduced with slightly lower wind speeds compared to neutral conditions (Figure 14). Far-wake spectra measured by the wls67 seem to have recovered to almost free stream conditions with a classical energy decay from lower to higher frequencies. The elevated variance of southerly winds has been smooth over a wider range of wind direction bins, including westerly winds. Data of wls37 and wls65 in unstable conditions show wake peak frequencies leaning towards lower values, but are too sparse for further interpretation.

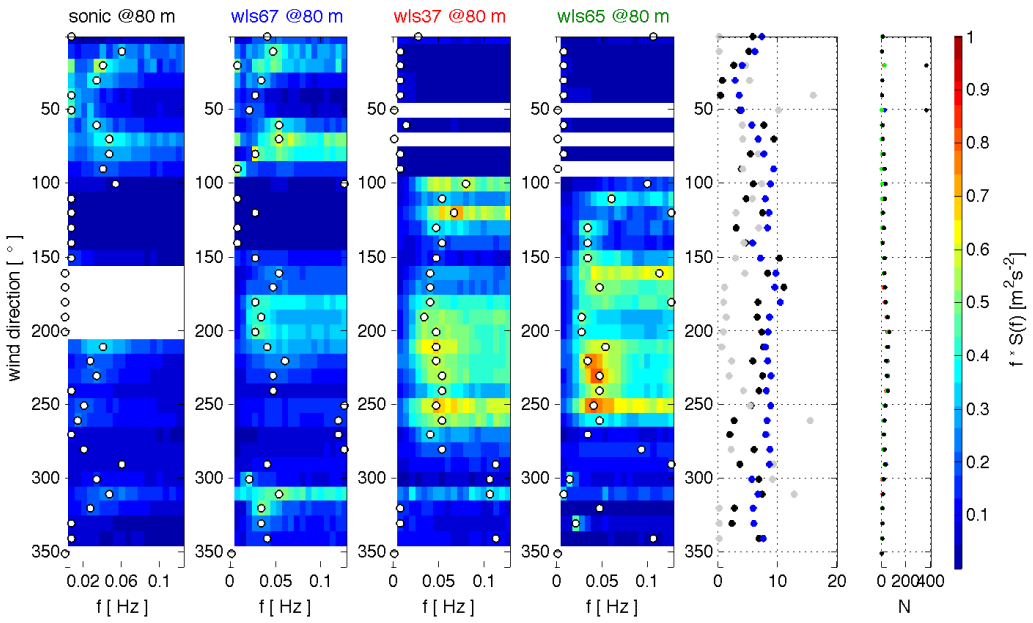

Figure 12. Composites of hourly energy spectra of u at 80 m for all wind direction bins from wls67, wls37 and wls65 (from left to right) filtered for stable wind conditions. White circles indicate the maximal spectral energy density of each direction bin. Additional subplots show wind direction bin averaged horizontal wind speeds at 108 m (blue in ($m \cdot s^{-1}$), power output (black in (MW/100)) and blade pitch angle (gray in (°)) of wind turbine WT6 and the number of averaged hours in each bin for wls67 (blue), wls37 (red) and wls65 (green).

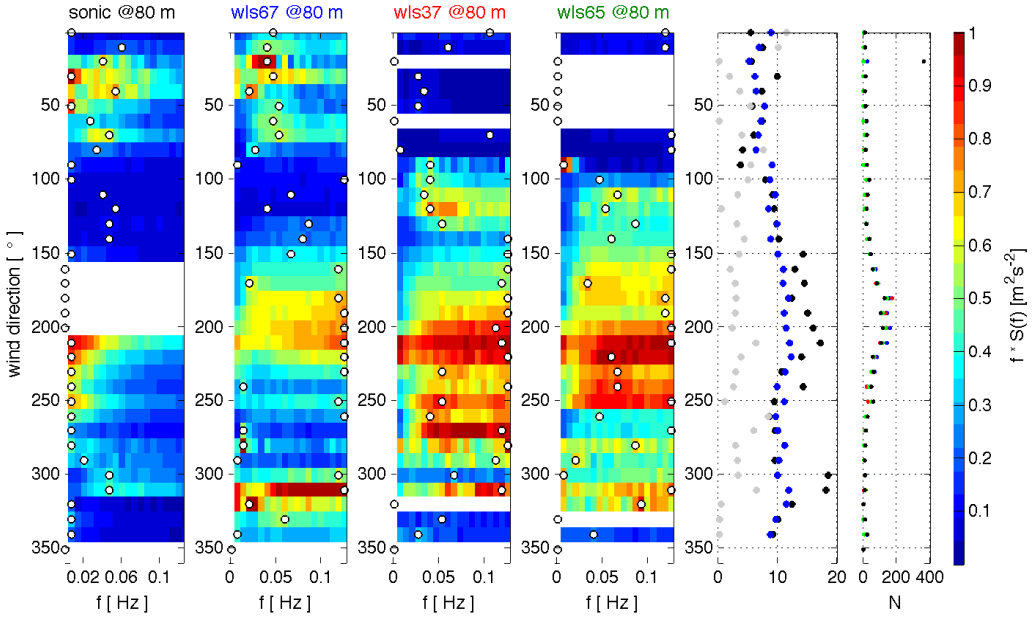

Figure 13. Composites of hourly energy spectra of u at 80 m for all wind direction bins from wls67, wls37 and wls65 (from left to right) filtered for neutral wind conditions. White circles indicate the maximal spectral energy density of each direction bin. Additional subplots show wind direction bin averaged horizontal wind speeds at 108 m (blue in ($m \cdot s^{-1}$)), power output (black in (MW/100)) and blade pitch angle (gray in (°)) of wind turbine WT6 and the number of averaged hours in each bin for wls67 (blue), wls37 (red) and wls65 (green).

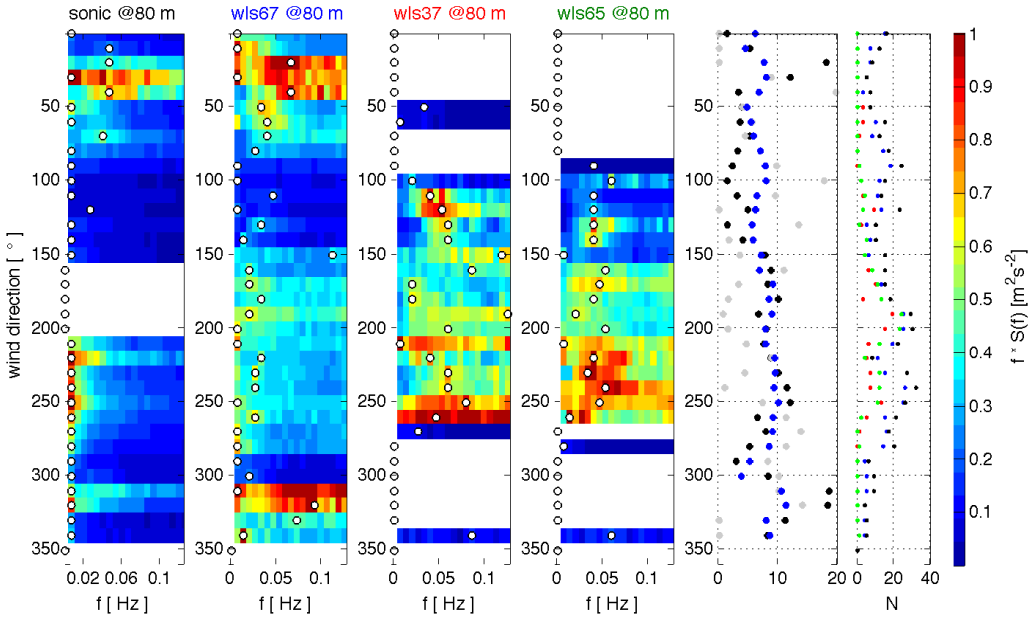

Figure 14. Composites of hourly energy spectra of u at 80 m for all wind direction bins from wls67, wls37 and wls65 (from left to right) filtered for unstable wind conditions. White circles indicate the maximal spectral energy density of each direction bin. Additional subplots show wind direction bin averaged horizontal wind speeds at 108 m (blue in ($m \cdot s^{-1}$)), power output (black in (MW/100)) and blade pitch angle (gray in (°)) of wind turbine WT6 and the number of averaged hours in each bin for wls67 (blue), wls37 (red) and wls65 (green).

4. Discussion

The above-presented wake spectra of the along-wind component u compare well with corresponding spectra presented by Højstrup [29]. Højstrup's study is based on cup anemometer measurements from two meteorological masts located in Nørrekær Enge II Windfarm in Denmark. The study presents a wake peak frequency of around 0.1 Hz at a 2 D downstream distance for wind speeds of 7 $m \cdot s^{-1}$. The turbines of the Nørrekær Enge II Windfarm are, with a rotor diameter of 28 m and a hub height of 31 m, much smaller than the turbines in Wieringermeer. The shift in the peak frequency from around 0.03 Hz in this study to 0.1 Hz for smaller turbines indicates a clear relationship between the rotor diameter and the wake peak frequency. Similar to Figure 9, the variance level drops almost back to free-stream conditions above blade tip height. The variance at hub height stays elevated, but broadens for higher wind speeds. Højstrup relates this broadening to wake meandering. This relation could also explain the broadening of the wake maximum observed in our upstream measurements, created by the meandering wake of the prototype turbines during stable conditions and the general broadening during neutral conditions, created by the meandering wake of the research turbines (Figure 11).

A wind tunnel study performed by Muller et al. [30] relates transverse velocity fluctuations to meandering by looking at the spectra of a horizontal wake position parameter, which the authors define in their study. The wind tunnel results during neutral conditions show a wake peak frequency in the u-spectra of $fD/u_{upstream} = 0.2$ at 5 D, which compares well to our results of $fD/u_{upstream} = 0.29$ during south-westerly winds of 11 $m \cdot s^{-1}$ at 3.2 D.

5. Conclusions

The study describes a spectral analysis of Windcube v1 DBS data in the vicinity of wind turbine wakes. Data originate from the WINTWEX-W measurement campaign performed at ECN's Wind Turbine Test Site Wieringermeer in the Netherlands. By filtering Windcube v1 DBS data as described in Section 2, we could retrieve energy spectra of the along wind component and of TKE that are in good agreement with spectra from sonic anemometer measurements and wind tunnel experiment. Cross-wind spectra show a higher sensibility to beam locations and wind direction variations, but further research needs to be done to better understand LiDAR cross-wind spectra. Improvements for the spectra of the vertical component could be reached with a Windcube v2, which directly measures vertical winds.

Despite the possible error source of probe volume averaging and the assumption of horizontal homogeneous flow, rotor-induced turbulences are captured and deliver information about wake peak frequencies dependent on prevailing stability conditions. Especially during stable conditions, wake effects are strongest, and different control strategies are needed. Improved control strategies could reduce the loads on wind turbines, as they are strongest during stable condition [31], and reduce the errors of annual energy production estimates, as the energy production is overestimated if stability conditions are not taken into account [32].

At offshore sites, wake recovery and wake-induced loads can become a greater issue since the surface roughness is decreased, leading to a less effective mixing, especially during stable conditions. Wake peak frequencies are of importance for load response studies, as offshore turbines are usually larger. Bigger rotors are more sensitive to horizontal flow inhomogeneity and larger-scale turbulent eddies. This can become an issue for future floating offshore wind parks, since the observed wake peak frequencies would interfere with the eigenfrequencies of the floater. However, offshore campaigns are needed to investigate potential differences between onshore and offshore wake characteristics in more detail.

Acknowledgments: The authors are very grateful to the Energy Centre of the Netherlands (ECN) for providing access to the test site Wieringermeer, in particular to Peter Eecen and Jan-Willem Waagenar for their help and support in planning and realizing the campaign. Special thanks to our colleagues Benny Svardal from Christian

Michelsen Research (CMR) and Gerben Bergman for their continuous efforts in installation, operation and data handling during and after the campaign.

The research presented in this study was supported by and conducted under the umbrella of the Norwegian Center for Offshore Wind Energy (NORCOWE), funded by the Research Council of Norway (RCN) under Project Number 193821. The majority of the mobile LiDAR instrumentation used during the WINTWEX-W campaign was made available by the national Norwegian Research Infrastructure project OBLO (Offshore Boundary Layer Observatory), also founded by RCN (Project Number 277770). The PhD project of the first author has been funded by the collaboration agreement between BKK (Bergenshalvøens Kommunale Kraftselskap) and the University of Bergen on renewable energy and energy transition.

Author Contributions: Valerie Kumer and Joachim Reuder conceived and designed the experiments. Valerie Kumer and Rannveig Oftedal Eikill analyzed the data. Valerie Kumer wrote the paper with input form Joachim Reuder and Rannveig Oftedal Eikill.

Conflicts of Interest: The authors declare no conflict of interest.

Abbreviations

The following abbreviations are used in this manuscript:

D	Rotor Diameter
DBS	Doppler Beam Swing
FINO	Forschungsplattform in Nord- und Ostsee
LiDAR	Light Detection and Ranging
RaDAR	Radio Detection and Ranging
SoDAR	Sonic Detection and Ranging
TI	Turbulence Intensity
TKE	Turbulent Kinetic Energy
WINTWEX-W	WINd Turbine Wake EXperiment Wieringermeer

References

1. Barthelmie, R.J.; Larsen, G.C.; Frandsen, S.T.; Folkerts, L.; Rados, K.; Pryor, S.C.; Lange, B.; Schepers, G. Comparison of Wake Model Simulations with Offshore Wind Turbine Wake Profiles Measured by Sodar. *J. Atmos. Ocean. Technol.* **2006**, *23*, 888–901.
2. Iungo, G.; Porté-Agel, F. Volumetric scans of wind turbine wakes performed with three simultaneous wind LiDARs under different atmospheric stability regimes. *J. Phys. Conf. Ser.* **2014**, *524*, 012164.
3. Trombe, P.J.; Pinson, P.; Vincent, C.; Bøvith, T.; Cutululis, N.A.; Draxl, C.; Giebel, G.; Hahmann, A.N.; Jensen, N.E.; Jensen, B.P.; et al. Weather radars—The new eyes for offshore wind farms? *Wind Energy* **2014**, *17*, 1767–1787.
4. Smalikho, I.N.; Banakh, V.A.; Pichugina, Y.L.; Brewer, W.A.; Banta, R.M.; Lundquist, J.K.; Kelley, N.D. Lidar Investigation of Atmosphere Effect on a Wind Turbine Wake. *J. Atmos. Ocean. Technol.* **2013**, *30*, 2554–2570.
5. Banakh, V.; Smalikho, I. *Coherent Doppler Wind Lidars in a Turbulent Atmosphere*; Artech House: London, UK, 2013.
6. Frehlich, R.; Meillier, Y.; Jensen, M.L.; Balsley, B.; Sharman, R. Measurements of boundary layer profiles in an urban environment. *J. Appl. Meteorol. Climatol.* **2006**, *45*, 821–837.
7. Krishnamurthy, R.; Calhoun, R.; Billings, B.; Doyle, J. Wind turbulence estimates in a valley by coherent Doppler LiDAR. *Meteorol. Appl.* **2011**, *18*, 361–371.
8. Barthelmie, R.J.; Crippa, P.; Wang, H.; Smith, C.M.; Krishnamurthy, R.; Choukulkar, A.; Calhoun, R.; Valyou, D.; Marzocca, P.; Matthiesen, D.; et al. 3D wind and turbulence characteristics of the atmospheric boundary layer. *Bull. Am. Meteorol. Soc.* **2014**, *95*, 743–756.
9. Mirocha, J.D.; Rajewski, D.A.; Marjanovic, N.; Lundquist, J.K.; Kosović, B.; Draxl, C.; Churchfield, M.J. Investigating wind turbine impacts on near-wake flow using profiling LiDAR data and large-eddy simulations with an actuator disk model. *J. Renew. Sustain. Energy* **2015**, *7*, 043143.
10. Aitken, M.L.; Banta, R.M.; Pichugina, Y.L.; Lundquist, J.K. Quantifying Wind Turbine Wake Characteristics from Scanning Remote Sensor Data. *J. Atmos. Ocean. Technol.* **2014**, *31*, 765–787.
11. Aitken, M.L.; Lundquist, J.K. Utility-scale wind turbine wake characterization using nacelle-based long-range scanning LiDAR. *J. Atmos. Ocean. Technol.* **2014**, *31*, 1529–1539.

12. Bingöl, F.; Mann, J.; Larsen, G.C. Light detection and ranging measurements of wake dynamics part I: One-dimensional scanning. *Wind Energy* **2010**, *13*, 51–61.
13. Sathe, A.; Banta, R.M.; Pauscher, L.; Vogstad, K.; Schlipf, D.; Wylie, S. *Estimating Turbulence Statistics and Parameters from Ground- and Nacelle-Based Lidar Measurements: IEA Wind Expert Report*; DTU Wind Energy: Roskilde, Denmark, 2015.
14. Kumer, V.M.; Reuder, J.; Dorninger, M.; Zauner, R.; Grubisic, V. Turbulent kinetic energy estimates from profiling wind LiDAR measurements and their potential for wind energy applications. *Renew. Energy* **2016**, *99*, 898–910.
15. Mann, J.; Cariou, J.P.; Courtney, M.S.; Parmentier, R.; Mikkelsen, T.; Wagner, R.; Lindelöw, P.; Sjöholm, M.; Enevoldsen, K. Comparison of 3D turbulence measurements using three staring wind LiDARs and a sonic anemometer. *Meteorol. Z.* **2009**, *18*, 135–140.
16. Fuertes, F.C.; Iungo, G.V.; Porte-Agel, F. 3D turbulence measurements using three synchronous wind LiDARs: Validation against sonic anemometry. *J. Atmos. Ocean. Technol.* **2014**, *31*, 1549–1556.
17. Rhodes, M.E.; Lundquist, J.K. The Effect of Wind-Turbine Wakes on Summertime US Midwest Atmospheric Wind Profiles as Observed with Ground-Based Doppler Lidar. *Bound.-Layer Meteorol.* **2013**, *149*, 85–103.
18. Kumer, V.M.; Reuder, J.; Svardal, B.; Sætre, C.; Eecen, P. Characterisation of Single Wind Turbine Wakes with Static and Scanning WINTWEX-W LiDAR Data. *Energy Procedia* **2015**, *80*, 245–254.
19. Lundquist, J.K.; Churchfield, M.J.; Lee, S.; Clifton, A. Quantifying error of LiDAR and sodar Doppler beam swinging measurements of wind turbine wakes using computational fluid dynamics. *Atmos. Meas. Tech.* **2015**, *8*, 907–920.
20. StatOil. *Hywind Scotland Pilot Park–Executive Summary of the Environmental Statement*; Technical Report; StatOil: Stavanger, Norway, 2015.
21. Schepers, J.G.; Obdam, T.S.; Prospathopoulos, J. Analysis of wake measurements from the ECN Wind Turbine Test Site Wieringermeer, EWTW. *Wind Energy* **2012**, *15*, 575–591.
22. Eikill, R. An Investigation of Single Wind Turbine Wakes with Static LiDAR Wind Profilers. Master's Thesis, University of Bergen, Bergen, Norway, 2016.
23. Sathe, A.; Mann, J.; Gottschall, J.; Courtney, M.S. Can Wind Lidars Measure Turbulence? *J. Atmos. Ocean. Technol.* **2011**, *28*, 853–868.
24. Canadillas, B.; Bégué, A.; Neumann, T. Comparison of turbulence spectra derived from LiDAR and sonic measurements at the offshore platform FINO1. In Proceedings of the 10th German Wind Energy Conference (DEWEK 2010), Bremen, Germany, 17–18 November 2010; pp. 18–21.
25. Sathe, A.; Mann, J. Measurement of turbulence spectra using scanning pulsed wind LiDARs. *J. Geophys. Res.: Atmos. (1984–2012)* **2012**, *117*, doi:10.1029/2011JD016786.
26. Fitch, A.C.; Olson, J.B.; Lundquist, J.K.; Dudhia, J.; Gupta, A.K.; Michalakes, J.; Barstad, I. Local and Mesoscale Impacts of Wind Farms as Parameterized in a Mesoscale NWP Model. *Mon. Weather Rev.* **2012**, *140*, 3017–3038.
27. Iungo, G.V.; Porté-Agel, F. Measurement procedures for characterization of wind turbine wakes with scanning Doppler wind LiDARs. *Adv. Sci. Res.* **2013**, *10*, 71–75.
28. Emeis, S. *Wind Energy Meteorology*; Springer: Berlin/Heidelberg, Germany, 2013; Volume 99, pp. 189–192.
29. Højstrup, J. Spectral coherence in wind turbine wakes. *J. Wind Eng. Ind. Aerodyn.* **1999**, *80*, 137–146.
30. Muller, Y.A.; Aubrun, S.; Masson, C. Determination of real-time predictors of the wind turbine wake meandering. *Exp. Fluids* **2015**, *56*, 53.
31. Sathe, A.; Mann, J.; Barlas, T.; Bierbooms, W.; van Bussel, G.J.W. Influence of atmospheric stability on wind turbine loads. *Wind Energy* **2013**, *16*, 1013–1032.
32. St. Martin, C.M.; Lundquist, J.K.; Clifton, A.; Poulos, G.S.; Schreck, S.J. Wind turbine power production and annual energy production depend on atmospheric stability and turbulence. *Wind Energ. Sci.* **2016**, *1*, 221–236.